The Influence of Divertor Plasma Parameter on Tungsten Screening in High Recycling Regime for CFETR

Guoliang Xu, Yifu Zhou, Shifeng Mao, Defeng Kong, Liu Li, Vincent Chan, and Minyou Ye

***Abstract*— Since tungsten is considered as the optional divertor target material for the future fusion devices, e.g., China Fusion Engineering Test Reactor (CFETR), it is crucial to have a good screening of the tungsten impurity to keep a low core tungsten concentration. In this paper, based on the two-point model, possible divertor plasma parameters are predicted in high recycling regime for CFETR. Further analysis of tungsten ionization lengths shows that when target temperature is low enough (less than 15 eV), the increase of upstream density may cause an increase of ionization length, and thus a degradation of divertor tungsten screening effect may happen. The 2-D simulations of tungsten transport are then performed by using Osm-Eirene-Divimp edGE [onion skin model (OSM)-EIRENE-DIVvertor IMPurities (DIVIMP)] code package. The target plasma parameters, in the region of those predicted by the two-point model, are set as input in OSM-EIRNEN to generate the background plasma. DIVIMP code is used to further simulate the tungsten impurity transport process. The results reveal that although the decrease of target plasma temperature may reduce the tungsten impurity prompt redeposition rate, the benefit of a lower erosion rate can make compensation. Therefore, to control the core tungsten concentration, lower target plasma temperature is preferred in high recycling regime.**

***Index Terms*— Impurity screening, ionization length, prompt redeposition, tungsten divertor, tungsten erosion.**

I. Introduction

COMPARED with low-Z plasma facing material, like carbon, tungsten has a lower sputtering yield and more importantly a lower tritium retention; thus, tungsten is chosen as the International Thermal Experiment Reactor (ITER) divertor material [1] and considered to be an important optional divertor target material for the future fusion devices, like the China Fusion Engineering Test Reactor (CFETR). CFETR is proposed to be a good complement of ITER to demonstration power plants [2]–[5]. Steady-state operation and demonstrating tritium self-sufficiency are the two main missions of CFETR. Taking advantage of the good thermomechanical property and low tritium retention, a full tungsten divertor design is beneficial for achieving these goals. Recent Joint European Torus (JET) ITER-like wall (tungsten divertor and beryllium first wall) experiment results showed that the fuel retention rate decreased by more than one order of magnetite compared with carbon wall [6], but tungsten core concentration may cause significant degradation of core performance simultaneously. Thus, understanding the tungsten impurity transport process and giving a preliminary assessment of the tungsten divertor influence are essential for the CFETR divertor design.

Unlike detached plasma condition, attached plasma condition has a relatively higher target temperature and will cause much higher target tungsten erosion. Therefore, the tungsten transport process under the attached divertor plasma conditions is worthful to study at.

Previous study [7] shows that the ionization length of neutral impurities created at the divertor target plane may play an important role in divertor impurity retention. If an impurity particle is ionized within a larmor radius from the target, it will have a great chance to prompt deposit on the target [8], thus increasing the divertor impurity retention. Because of this, evaluating the neutral tungsten ionization length will be the first step to predict the divertor impurity retention.

The Osm-Eirene-Divimp edGE (OEDGE) [onion skin model (OSM)-EIRENE-DIVvertor IMPurities (DIVIMP)] code [9] package is employed, where OSM-EIRENE provides 2-D scrape-off layer (SOL) plasma background, and DIVIMP [10] code simulates the impurity distribution. Unlike other 2-D fluid codes, the OSM treats the cross-field transport in a rough way, solves 1-D fluid equations for different flux tubes, and thus gets the 2-D edge plasma [11]. Since it is relatively less time consuming, it is good for preliminary parameter scanning work.

In this paper, the CFETR high recycling operation regimes are predicted by the two-point model [11]–[13], and a comparison of W^0 ionization length with the larmor radius is carried out in Section II. In Section III, the OEDGE calculation

Manuscript received June 30, 2017; revised October 12, 2017; accepted November 15, 2017. Date of publication March 23, 2018; date of current version May 8, 2018. This work was supported in part by the National Natural Science Foundation of China under Grant 11375191 and in part by the National Magnetic Confinement Fusion Science Program of China under Grant 2014GB110001, Grant 2014GB110002, and Grant 2014GB110003. The review of this paper was arranged by Senior Editor E. Surrey. *(Corresponding author: Minyou Ye.)*

G. L. Xu and V. Chan are with the School of Physical Sciences, University of Science and Technology of China, Hefei 230026, China, and also with General Atomics, San Diego, CA 92186-5608 USA (e-mail: xudaren@mail.ustc.edu.cn; chanvs@ustc.edu.cn).

Y. Zhou, S. Mao, and L. Li are with the School of Physical Sciences, University of Science and Technology of China, Hefei 230026, China (e-mail: zhouyifu@mail.ustc.edu.cn; sfmao@ustc.edu.cn; liuli92@mail.ustc.edu.cn).

D. Kong is with the Institute of Plasma Physics, Chinese Academy of Sciences, Hefei 230031, China (e-mail: dfkong@ipp.ac.cn).

M. Y. Ye is with the School of Physical Sciences, University of Science and Technology of China, Hefei 230026, China, and also with the Institute of Plasma Physics, Chinese Academy of Sciences, Hefei 230031, China (e-mail: yemy@ustc.edu.cn).

Color versions of one or more of the figures in this paper are available online at http://ieeexplore.ieee.org.

Digital Object Identifier 10.1109/TPS.2017.2776227

details are introduced. Section IV contains the OEDGE calculation results and a discussion, followed by a conclusion in Section V.

II. Analysis Based on Two-Point Model

Two-point model is widely used to give a prediction of target plasma parameters for different upstream conditions. From the basic two-point model [11] for the significant parallel temperature gradient cases, the target plasma temperature and density can be expressed by

$$T_{t0} = 2.67 \times 10^{-3} \left(\frac{m_i}{\gamma^2 e^{37/9}}\right) \times \left(\frac{P_{\rm SOL}^{20/9} \kappa_0^{8/9}}{\left(n_u^{\rm sep}\right)^{28/9} \left(\chi_\perp^{\rm SOL}\right)^{10/9} L^{8/9} (B_\theta/B)_u^{7/9} R^{14/9} a^{7/9}}\right) \quad (1)$$

$$n_{t0} = 82.2 \left(\frac{\gamma^2 e^{35/9}}{m_i}\right) \times \left(\frac{\left(n_u^{\rm sep}\right)^{35/9} \left(\chi_\perp^{\rm SOL}\right)^{8/9} L^{10/9} (B_\theta/B)_u^{8/9} R^{16/9} a^{8/9}}{P_{\rm SOL}^{16/9} \kappa_0^{10/9}}\right) \quad (2)$$

where m_i is the mass of main ion, γ is the sheath heat transmission coefficient, $\gamma = 7$, $e = 1.6 \times 10^{19}$, κ_0 is the electron parallel conductivity coefficient, $\kappa_0 = 2000$, $\chi_\perp^{\rm SOL}$ is the cross-field energy transport coefficient, $\chi_\perp^{\rm SOL} = 4$ m^2/s, $L = 120$ m is the magnetic connect length from the target to the outer midplane, B_θ is the poloidal magnetic field, B is the total magnetic field, the subscript u means at the upstream (outer midplane), R is the major radius, $R = 5.6$ m, and a is the minor radius, $a = 1.6$ m. $P_{\rm SOL}$ is the total energy into the SOL, and $n_u^{\rm sep}$ is the upstream density.

If the SOL radiation loss is taken into consideration, the target temperature and density should be multiplied by a factor of $(1 - f_{\rm rad})^2$ and $(1 - f_{\rm rad})^{-2}$, respectively [12], [13], where $f_{\rm rad}$ is the ratio of radiated power over the total power into SOL, assumed to be 0.8 in this paper, thus

$$T_t = (1 - f_{\rm rad})^2 T_{t0} \quad (3)$$

$$n_t = (1 - f_{\rm rad})^{-2} n_{t0}. \quad (4)$$

For given $P_{\rm SOL}$ and $n_u^{\rm sep}$, we can get the plasma temperature and density at the target, and then calculate the W^0 ionization length by using

$$l_i = \frac{V_{\rm in}}{\kappa n_t}. \quad (5)$$

$V_{\rm in}$ is the initial neutral tungsten velocity and κ is the W^0 ionization rate taken from ADPAK database [14]. In a detailed 2-D simulation in Section III, $V_{\rm in}$ is sampled according to

$$V_{\rm in} = \sqrt{\frac{2E_{\rm bd}}{m_i}} \left(\frac{1}{\sqrt{x}} - 1\right) \quad (6)$$

where $E_{\rm bd} = 8.68$ eV is tungsten surface binding energy and x is a random number in the range of (0, 1).

For simple analysis, $V_{\rm in}$ is set as average velocity $(2E_{\rm bd}/m_i)^{1/2}$.

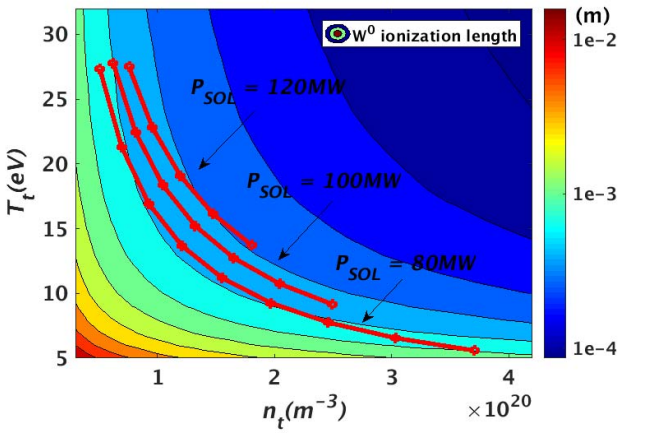

Fig. 1. W^0 ionization length for different divertor target plasma conditions.

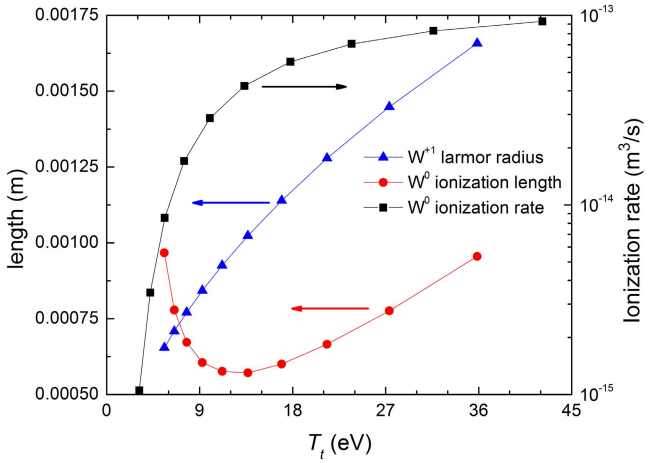

Fig. 2. W^0 ionization length, W^{+1} larmor radius, and W^0 ionization rate for different divertor target plasma temperatures of $P_{\rm SOL} = 80$-MW operation regime.

The power into SOL for CFETR cases is about 100 MW. For a fixed $P_{\rm SOL}$, different target plasma parameters can be achieved by varying upstream density from 1×10^{19} m^{-3} to 4×10^{19} m^{-3}. Fig. 1 shows the possible target plasma conditions of high recycling operation regimes and corresponding W^0 ionization lengths for the $P_{\rm SOL}$ set as 80, 100, and 120 MW separately. Increasing the upstream density can help to achieve a lower target plasma temperature and thus lower the tungsten sputtering yields. For the $P_{\rm SOL}$ equals 120- and 100-MW cases, increasing upstream density can also help to achieve a short W^0 ionization length, which is helpful to stop tungsten from transport to the core plasma by increasing the tungsten prompt redeposition probability. But for the $P_{\rm SOL}$ equals 80-MW cases, with the target plasma density going up, the W^0 ionization length decrease first then increase.

Fig. 2 shows the comparison of W^0 ionization length with the larmor radius of W^{+1} under the possible target plasma conditions of $P_{\rm SOL} = 80$ MW. The larmor radius of W^{+1} near the target can be expressed by

$$L_l = \frac{m_i c_s}{B_t} \quad (7)$$

where c_s is the W^{+1} sound speed and B_t is the magnetic field at the target. If the ionization length is less than the

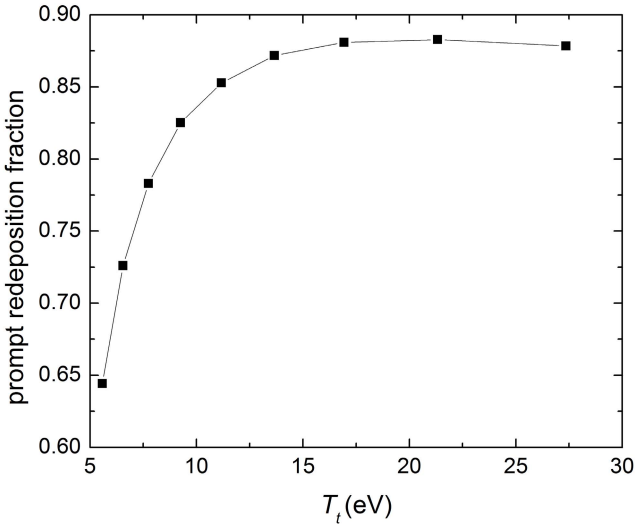

Fig. 3. Prompt redeposition rate for different divertor target plasma temperatures of $P_{\mathrm{SOL}} = 80$ MW operation regime.

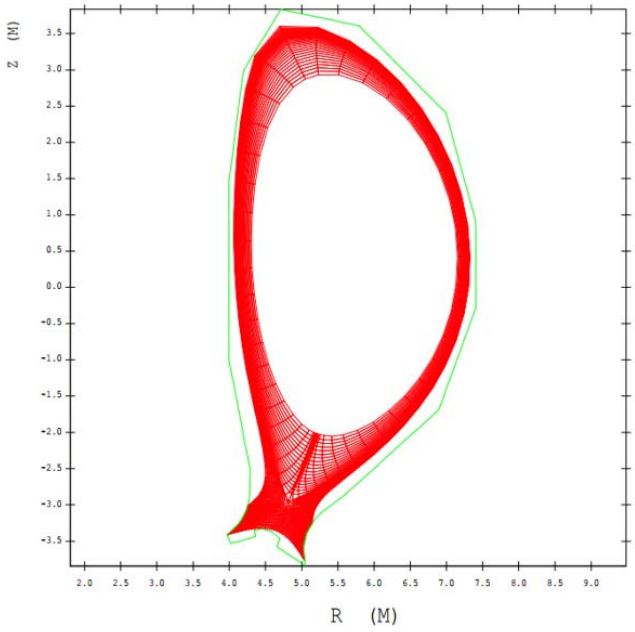

Fig. 4. First wall and grid geometry used in this paper. It is a lower single null CFETR geometry shape with an ITER-like divertor.

W^{+1} larmor radius, the ionized tungsten will be considered to be prompt redeposit on the target. With the target plasma temperature decreasing, the W^{+1} larmor radius decreases, and the W^0 ionization length decreases first then increases when the temperature is less than 15 eV. It is because the ionization length is dominated by the fast decreasing ionization rate when the temperature is below 15 eV rather than the increasing density, as shown in Fig. 2.

The increasing of W^0 ionization length at the low target plasma temperature may encounter a degradation of divertor tungsten screening effect. To evaluate the tungsten prompt redeposition rate, the initial velocity of neutral tungsten is assumed to follow the distribution of function (6). By comparing the neutral tungsten ionization length with W^{+1} larmor radius, the prompt redeposition rate can be estimated. As shown in Fig. 3, the decrease of target plasma temperature may reduce the tungsten impurity prompt redeposition rate by more than 20 percent. Although a lower target plasma temperature is expected to help to achieved a lower tungsten erosion rate, the lower prompt deposition rate may bring some adverse effect. To evaluate the influence of this phenomenon, 2-D calculation is carried out.

III. OEDGE Calculation Details

A. Geometry

The first wall and grid geometry are shown in Fig. 4. It is a lower single null CFETR geometry shape with an ITER-like divertor. The major radius and minor radius are 5.6 and 1.6 m, respectively. The toroidal field on the magnetic axis is 5 T. The grid can be divided into two parts. The edge region, $0.9 < r/a < 1$, contains the pedestal information, and the SOL region, $r/a > 1$, contains the scrap of layer information.

B. Background Plasma and Impurity Transport

The background hydric plasma in the region $0.9 < r/a < 1$ is taken from EPED simulation with the pedestal top density set to be 8×10^{19} m^{-3}. To generate a set of SOL plasma ($r/a > 1$), some assumptions are made.

1) Electron and ion temperature at the target are the same, $T_{i\_\mathrm{target}} = T_{e\_\mathrm{target}}$.
2) Heat flux, density, and temperature peak at the strike point and exponentially decay along the target.

The strike point density and temperature are chosen from the high recycling operation lines predicted in Fig. 1. For each P_{SOL} value, five target conditions are chosen and listed as different cases in Table I.

The SOL energy decay length implied in the two-point model in Section II is expected as

$$\lambda_q = 0.0161\left(\frac{P_{\mathrm{SOL}}^2}{en_u^{\mathrm{sep}}\chi_\perp^{\mathrm{SOL}}}\right)^{7/9}\frac{\kappa_0^{2/9}}{L^{2/9}(B_\theta/B)_u^{7/9}R^{14/9}a^{7/9}}. \quad (8)$$

From the relationship among heat flux, density, and temperature decay lengths in the SOL region [11]

$$\lambda_q = \left(\frac{1.5}{\lambda_T} + \frac{1}{\lambda_n}\right)^{-1} \quad (9)$$

$$\lambda_n = 1.4\lambda_T. \quad (10)$$

We can get

$$\lambda_T = 2.21\lambda_q \quad (11)$$

$$\lambda_n = 3.09\lambda_q. \quad (12)$$

Thus, the temperature and density decay lengths at the target should be

$$\lambda_{Tt} = \lambda_T f\cos\theta = 2.21\lambda_q f\cos\theta \quad (13)$$

$$\lambda_{nt} = \lambda_n f\cos\theta = 3.09\lambda_q f\cos\theta \quad (14)$$

where f is the magnetic flux expansion, θ is the angle between the magnetic field line and the target's normal. f and θ are 2.6, and 5°, respectively.

TABLE I
TARGET CONDITIONS FOR DIFFERENT P_{SOL}

P_{sol} (MW)	case 1		case 2		case 3		case 4		case 5	
	n_t (10^{20}/m^3)	T_t (eV)	n_t (10^{20}/m^3)	T_t (eV)	n_t (10^{20}/m^3)	T_t (eV)	n_t (10^{20}/m^3)	T_t (eV)	n_t (10^{20}/m^3)	T_t (eV)
80	0.51	27.36	0.93	16.93	1.56	11.18	2.46	7.75	3.70	5.58
100	0.62	27.81	0.81	22.43	1.32	15.20	2.04	10.75	2.49	9.17
120	0.76	27.52	0.96	22.79	1.20	19.08	1.48	16.12	1.80	13.75

TABLE II
TUNGSTEN CONCENTRATION INSIDE OF THE SEPARATRIX

Tungsten Concentration	P_{SOL} = 80 MW	P_{SOL} = 100 MW	P_{SOL} = 120 MW
case 1	2.29×10^{-7}	1.83×10^{-7}	1.45×10^{-7}
case 2	6.24×10^{-8}	9.37×10^{-8}	8.29×10^{-8}
case 3	8.07×10^{-9}	2.09×10^{-8}	4.28×10^{-8}
case 4	1.60×10^{-9}	6.26×10^{-9}	3.08×10^{-8}
case 5	5.25×10^{-10}	2.04×10^{-9}	1.60×10^{-8}

With the assumption listed above and density and temperature at the strike point, the plasma density, and temperature profiles at the target can be generated. Then by using the OSM, different SOL background plasmas can be generated. To compare with the prediction result in Section II, the radiation ratio in the OSM is also set to be 0.8.

The radiation power is assumed mainly due to neon impurity. In this paper, the neon concentration at the separatrix is fixed to 0.5% [15] to calculate the tungsten sputtering yields. Then the DIVIMP code launches the tungsten impurity from the targets and traces the transport process in the background plasma. Tungsten self-sputtering part is self consistently calculated in the code.

IV. RESULTS AND DISCUSSION

Since the cross-field transport model in DIVIMP is not sufficient to give an accurate tungsten distribution in the core, the tungsten concentration just inside of the separatrix is chosen to evaluate the tungsten core concentration. The tungsten concentrations inside of the separatrix calculated by using OEDGE code package for the cases in Table I are listed in Table II. The results reveal that a lower target plasma temperature can always help to achieve a lower tungsten concentration inside of the separatrix and thus get a lower tungsten core concentration for different P_{SOL} cases. For all these cases, relatively low tungsten concentrations are achieved, because of the low tungsten erosion rate [showed in Fig. 5(b)]. For such low temperature, the tungsten erosion rate should be dominated by the neon distribution. Therefore, simulation by impurity seeding from edge rather than the specified neon concentration would give a more reasonable neon distribution, and then the tungsten erosion rate. Since this paper mainly focuses on the target plasma condition's influence on the tungsten screening effect, the influence of neon distribution will not be discussed here.

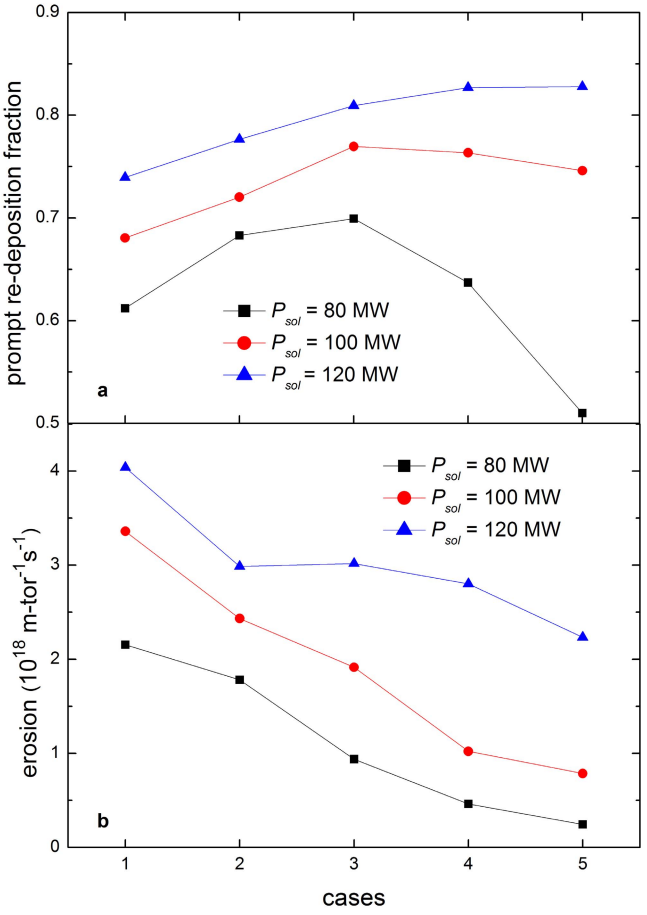

Fig. 5. Prompt redeposition and total erosion for different cases. (a) Prompt redeposition fraction lines for different P_{SOL} cases. A roll over happened for the P_{SOL} equals 80-MW cases. (b) Total tungsten erosion lines for different P_{SOL} cases, the unit m-tor^{-1}s^{-1} means per meter toroidal and second.

The tungsten concentration inside of the separatrix is mainly determined by two key parameters: the total tungsten erosion and divertor tungsten screening effect, i.e., the ratio of tungsten particles which can transport to the core to the total erosion. From the two-point model prediction in Section II, the increase of upstream density is expected to get a lower tungsten concentration inside of the separatrix for P_{SOL} equals 100- and 120-MW cases. But for the P_{SOL} equals 80-MW cases, when increase the upstream density, a target plasma temperature lower than 15 eV can be achieved.

And then the increase of neutral tungsten ionization length may play an important role in reduce the prompt redeposition ratio thus cause a degradation of divertor tungsten screening effect. Similar results are got from DIVIMP calculation. As shown in Fig. 5(a), the prompt redeposition ratios of P_{SOL} equals 80-MW cases encounter a roll over as targets plasma temperature decreasing. Compare the P_{SOL} equals 80-MW line with the simple model prediction in Fig. 3, the simple model prediction is overestimated. That is because the simple model's result is a prediction of the strike point, but the DIVIMP results is an average of the whole target. The whole target has a relatively lower temperature and density, thus has a longer W^0 ionization length and a lower prompt redeposition rate.

The prompt redeposition fraction decreases by about 0.2 when the temperature changes from 11.18 eV (case 3) to 5.58 eV (case 5) as predicted by the simple model in Section II, whereas the total tungsten erosion decreased by a factor of 4 for the same two cases, as shown in Fig. 5(b). Therefore, if the total erosion is taken into consideration, the decrease of target plasma temperature will be accompanied by a decrease of total tungsten erosion, and compared to the degradation of screening effect, the benefit of erosion decrease is proven to be more important. As a result, for different P_{SOL} values, increasing the upstream density is always beneficial for achieving a low tungsten core concentration.

V. Conclusion

Possible divertor plasma parameters are predicted for high recycling operation of CFETR by the two-point model with different P_{SOL} and upstream densities. A comparison of W^0 ionization length for the different divertor target conditions reveals that the impurity prompt redeposition ratio may become lower thus brings an unfavorable effect on the tungsten impurity control when the target plasma temperature is lower than 15 eV. To assess the tungsten screening effect, 2-D calculation is carried out for the cases predicted by the two-point model. The results showed the prompt deposition rate is in reasonable agreement with that derived from two-point model while the 2-D temperature and density distribution are included. However, if the benefits of lower erosion rate for the lower temperature cases are taken into consideration, a lower temperature, in other words, increasing the upstream density under fixed P_{SOL}, can always help to achieve a lower tungsten core concentration.

The OEDGE package is widely used to simulate the tungsten distribution for different Tokamaks, such as ASDEX-U [16], JET [17], and DIII-D [18], and can achieve a good agreement with experimental data. Nevertheless, since the background plasma generated by OSM is set to be fixed regardless of the impurity distribution, it may bring some inaccuracy for prediction work. Moreover, the prompt redeposition model in the DIVIMP code is very simple which does not include the sheath information, whereas the variation of density inside of the sheath is proven to be important to affect the neutral tungsten ionization process [19]. Therefore, a feedback progress between OSM and DIVIMP to consider the impurity influence on the background plasma and a more accurate sheath model need to be developed in the future work.

Acknowledgment

The authors would like to thank Dr. D. Rui for his valuable discussions and suggestion. They also would like thank the University of Toronto Institute for Aerospace Studies, Toronto, ON, Canada, for permission to use the OEDGE code for their valuable technical support.

References

[1] T. Hirai *et al.*, "ITER tungsten divertor design development and qualification program," *Fusion Eng. Des.*, vol. 88, nos. 9–10, pp. 1798–1801, 2013.

[2] B. Wan, S. Ding, J. Qian, G. Li, B. Xiao, and G. Xu, "Physics design of CFETR: Determination of the device engineering parameters," *IEEE Trans. Plasma Sci.*, vol. 42, no. 3, pp. 495–502, Mar. 2014.

[3] V. S. Chan, A. E. Costley, B. N. Wan, A. M. Garofalo, and J. A. Leuer, "Evaluation of CFETR as a fusion nuclear science facility using multiple system codes," *Nucl. Fusion*, vol. 55, no. 2, p. 023017, 2015.

[4] Y. T. Song *et al.*, "Concept design of CFETR tokamak machine," *IEEE Trans. Plasma Sci.*, vol. 42, no. 3, pp. 503–509, Mar. 2014.

[5] Z. Luo, B. Xiao, Y. Guo, and M. Ye, "Concept design of optimized snowflake diverted equilibria in CFETR," *IEEE Trans. Plasma Sci.*, vol. 42, no. 4, pp. 1021–1025, Apr. 2014.

[6] S. Brezinsek *et al.*, "Fuel retention studies with the ITER-like wall in JET," *Nucl. Fusion*, vol. 53, no. 8, p. 083023, 2013.

[7] P. C. Stangeby and J. D. Elder, "Impurity retention by divertors. I. One dimensional models," *Nucl. Fusion*, vol. 35, no. 11, p. 1391, 1995.

[8] A. Järvinen *et al.*, "DIVIMP simulation of W transport in the SOL of JET H-mode plasmas," *Phys. Scripta*, vol. 2011, no. T145, p. 014013, 2011.

[9] P. Stangeby *et al.*, "Interpretive modeling of simple-as-possible-plasma discharges on DIII-D using the OEDGE code," *J. Nucl. Mater.*, vol. 313, pp. 883–887, 2003.

[10] P. C. Stangeby and J. D. Elder, "Calculation of observable quantities using a divertor impurity interpretive code, DIVIMP," *J. Nucl. Mater.*, vols. 196–198, pp. 258–263, Dec. 1992.

[11] P. C. Stangeby, *The Plasma Boundary of Magnetic Fusion Devices*. Bristol, U.K.: Institute of Physics Publishing, 2000.

[12] V. Kotov and D. Reiter, "Two-point analysis of the numerical modelling of detached divertor plasmas," *Plasma Phys. Control. Fusion*, vol. 51, no. 11, p. 115002, 2009.

[13] P. C. Stangeby and C. Sang, "Strong correlation between D_2 density and electron temperature at the target of divertors found in SOLPS analysis," *Nucl. Fusion*, vol. 57, no. 5, p. 056007, 2017.

[14] K. Asmussen *et al.*, "Spectroscopic investigations of tungsten in the EUV region and the determination of its concentration in tokamaks," *Nucl. Fusion*, vol. 38, no. 7, p. 967, 1998.

[15] B. Braams, "Radiative divertor modelling for ITER and TPX," *Contrib. Plasma Phys.*, vol. 36, nos. 2–3, pp. 276–281, 1996.

[16] K. Krieger *et al.*, "Modelling of impurities in the ASDEX-Upgrade divertor with DIVIMP," *J. Nucl. Mater.*, vols. 220–222, pp. 548–552, Apr. 1995.

[17] S. K. Erents *et al.*, "Assessment of the DIVIMP 'onion-skin' model in the JET Mark I divertor," *J. Nucl. Mater.*, vols. 241–243, pp. 433–437, Feb. 1997.

[18] T. Abrams *et al.*, "The inter-ELM tungsten erosion profile in DIII-D H-mode discharges and benchmarking with ERO+OEDGE modeling," *Nucl. Fusion*, vol. 57, no. 5, p. 056034, 2017.

[19] R. Ding *et al.*, "Simulation of gross and net erosion of high-Z materials in the DIII-D divertor," *Nucl. Fusion*, vol. 56, no. 1, p. 016021, 2016.

Authors' photographs and biographies not available at the time of publication.